

Spot-profile-analyzing LEED study of the epitaxial growth of Fe, Co, and Cu on Cu(100)

G. L. Nyberg,* M. T. Kief, and W. F. Egelhoff, Jr.

Surface and Microanalysis Science Division, National Institute of Standards and Technology, Gaithersburg, Maryland 20899

(Received 20 May 1993)

The structure of epitaxial films of Fe, Co, and Cu grown at 80–300 K on Cu(100) has been investigated using a spot-profile-analyzing low-energy electron-diffraction (LEED) instrument. In all three systems rings appear around the substrate LEED spots, although the rings differ in intensity and in diameter depending upon the variables of film thickness and deposition temperature. Rings of this type have been studied extensively by Henzler *et al.* and correlated with the mean separation between islands. Much can be inferred about the growth mechanism through a study of these Henzler rings. The rings contract radially with increasing deposition temperature or with increasing annealing temperature as thermally activated diffusion permits the formation of larger islands with greater distances between them. For all three systems studied here, the onset of thermal diffusion becomes apparent as the ring contracts radially for deposition temperatures above about 150 K. However, for deposition at 80 K, where thermally activated diffusion should be completely suppressed, rings are observed with a radius corresponding to a mean separation between islands on the order of ten atoms. Of the three elements, Fe gives the strongest rings and Cu the weakest. The value of the mean separation suggests that upon condensation these atoms do not come to rest at the immediate site of impact but instead experience some very transient type of mobility associated with the impact and accommodation process.

I. INTRODUCTION

The study of imperfections at crystal surfaces by low-energy electron diffraction (LEED) has a long history, being one of the classic problems of surface science.^{1–53} Following the early recognition of the relationship between LEED spot broadening or splitting and imperfections, such as steps, at the surface,^{1–5} much work was devoted to putting this qualitative understanding on a firm theoretical foundation.^{5–31} At present a reasonably clear understanding of this relationship is possible, and a number of review articles are available.^{8,13,20,23,24,31,39,40} Over the years, high-resolution, automated LEED instruments were developed to facilitate such measurements.^{22,32–37}

The broadening or splitting of LEED spots is particularly powerful as a diagnostic of epitaxial growth.^{12,13,20–22,27,28,38,40,44,52,53} Surface structural characteristics such as regular or random steps, regular or random island size or island spacing, regular or irregular island shape, the presence or absence of facets or mosaic structure, superstructures, point defects, strain, step heights, etc., can often be identified and measured quantitatively. The insights provided by such measurements are particularly valuable if they are systematically correlated with a variation of epitaxial growth conditions such as growth temperature or appealing temperature. Such correlations can provide much insight into the microscopic atomic dynamics of epitaxial growth mechanisms.

A variant on the theme of broadening and splitting of LEED spots is the rings that sometimes appear around the spots during the course of epitaxial growth. The pioneering work on these rings was done by Henzler and co-workers who have demonstrated that these rings are an indication of the nucleation and growth of islands dur-

ing epitaxy.^{12,13,15,22,24,47} The radius of these “Henzler” rings is reciprocally related to the characteristic separation between islands (center to center). Asymmetries in the ring can be related to island shape, and the variations in the radius with deposition temperature or annealing temperature can provide much insight into surface diffusion processes.^{12,13,15,22,24,47,54–56} In the present paper our major aim is to present the results of our studies of the Henzler rings that we have found in the systems Fe, Co, and Cu on Cu(100) and to discuss the implications these results have for the microscopic atomic dynamics of epitaxial growth mechanisms.

One issue of current interest in epitaxy concerns the dynamics of the impact and accommodation processes when a deposited atom lands on a crystal surface. It might seem that one of the simplest questions would be whether the atom, as it accommodates thermally with the surface during the first picosecond or so after impact, can hop around on the surface as the heat of condensation is released. Since the heat of condensation is often an order-of-magnitude larger than the activation energy for thermally activated surface diffusion, such mobility may be possible. The testing ground for such questions is, in general, epitaxy at cryogenic substrate temperatures in order to suppress thermally activated diffusion, although in some cases inferences can be drawn from growth at higher temperatures on the basis of wide variations in deposition rates.⁵⁷

At present, there is no clear consensus in the literature about whether some type of mobility associated with the dissipation of the heat of condensation is the rule or the exception during impact and accommodation processes. Experimental data [from LEED, reflection high-energy electron diffraction (RHEED), low-energy ion scattering, and field ion microscopy] have been presented on both

sides of the issue, with indications that such mobility does not occur in the W/W(100) system⁵⁸ or the Pd/Pd(100) system,⁵⁹ and that such mobility does occur in the Fe and Cu on Ag(100) and Cu(100) systems,⁶⁰ the In/Cu(100) system,⁶¹ and the Ag/Si(111) system.⁵⁷ However, these results are perhaps more suggestive than conclusive. Theoretical modeling of the accommodation process by molecular-dynamics simulations gives mixed results⁶²⁻⁶⁷ which appear to be very sensitive to the choice of parameters and are therefore also perhaps more suggestive than conclusive. Results that do seem conclusive have come from scanning tunneling microscopy (STM) studies of Xe on Pt(111) at 4 K.⁶⁸ The STM work shows that the Xe atoms travel hundreds of angstroms across the surface during the process of thermal accommodation before they come to rest.⁶⁸

With this material as a background, it seems both interesting and timely to undertake spot-profiling-analyzing (SPA) -LEED studies of the structure of epitaxial films grown at cryogenic substrate temperatures. Moreover, a SPA-LEED study of the growth of Fe, Co, and Cu on Cu(100) is particularly appropriate in light of the recent discovery of the "giant magnetoresistance" (GMR) effect and of oscillatory antiferromagnetic (AF) coupling in superlattices consisting of alternating films of these elements.⁶⁹ Many of the most important questions about the GMR effect and AF coupling are concerned with the structure and growth of such films.⁷⁰ The present results help to fill some of the gaps in present knowledge on these matters.

II. EXPERIMENT

The experimental apparatus used in this work has been largely described elsewhere,⁷¹ and only a brief summary will be given here. A sample preparation chamber with a base pressure of 2×10^{-10} Torr was equipped with four homemade metal evaporators. Deposited thicknesses were monitored with two quartz-crystal-oscillator thin film thickness monitors located immediately adjacent to the sample. These monitors were calibrated using reflection high-energy electron-diffraction (RHEED) oscillation period, and the agreement between the manufacturer's calibration and oscillation period was

within $\pm 5\%$.⁶⁰ Sample cleanliness was checked with x-ray photoelectron spectroscopy which has a detection threshold of $\sim 1\%$ of a monolayer of carbon or oxygen contamination. The Cu(100) crystal was cut with a wire-slurry saw, aligned within $\pm 0.25^\circ$ with an x-ray diffractometer, and polished by an acid-etch technique described earlier.⁷² The diffractometer indicated that the crystal was twinned with a minor grain (accounting for approximately 20% of the volume) being misoriented by $\sim 1^\circ$. Such low-angle twins are common in the Bridgeman-grown Cu crystals sold commercially. The sample temperature was monitored with a W-3%Re/W-25%Re thermocouple spot welded directly to the sample. The thermocouple was calibrated to within ± 1 K at 77 K by immersing the mounted sample in liquid nitrogen.

The new aspect of the present apparatus consists of the addition of a SPA-LEED instrument. Figure 1 presents a schematic illustration of this instrument. All data reported here were recorded by pulse counting the electrons as the octapole deflection plates swept a LEED spot or spots across the multiplier. This method of collecting data has several advantages. It avoids any possible problems with linearity of phosphor screens, vidicon tubes, or spot photometers. It permits rapid collection of data, and because of the very low beam currents, no detectable sample heating occurs. All data were collected within a few degrees of normal incidence, as Fig. 1 suggests.

One advantage in using a SPA-LEED instrument, as opposed to conventional instruments, is the ease with which the most nearly perfect regions of a sample can be selected for study. The speed of data collection and the contour-plot mode of data presentation permit an unusually detailed analysis of crystalline state at a great variety of locations on the surface. Figure 2 provides an illustration of the type of imperfections that may be found. In the sequence from 2(a)-2(d) the sample was translated so that the beam crosses a low-angle grain boundary of the type often observed in the common Bridgeman-grown commercial Cu single crystals. In addition to this twinning effect, the high resolution and wide dynamic range of the SPA-LEED instrument permits the detection of more subtle surface imperfections associated with the mosaic structure of the substrate and with faceting of small portions of the surface.^{24,34,47} Another subtlety is elongation of spots, which is an indication of limits to the

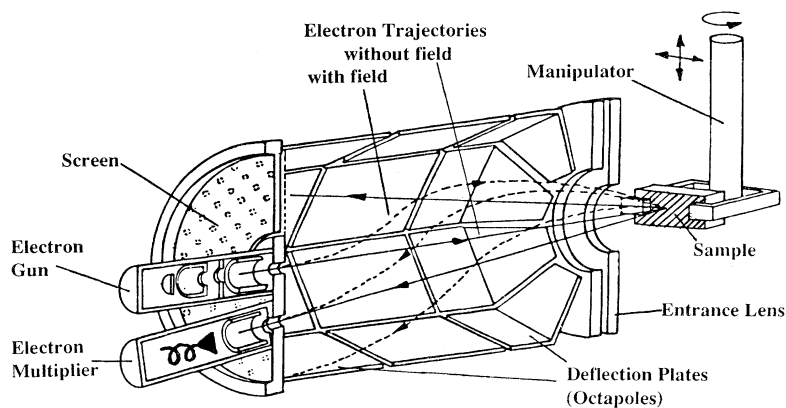


FIG. 1. A cut-away illustration of the interior of the SPA-LEED instrument indicating the electron trajectories with and without the applied deflection field.

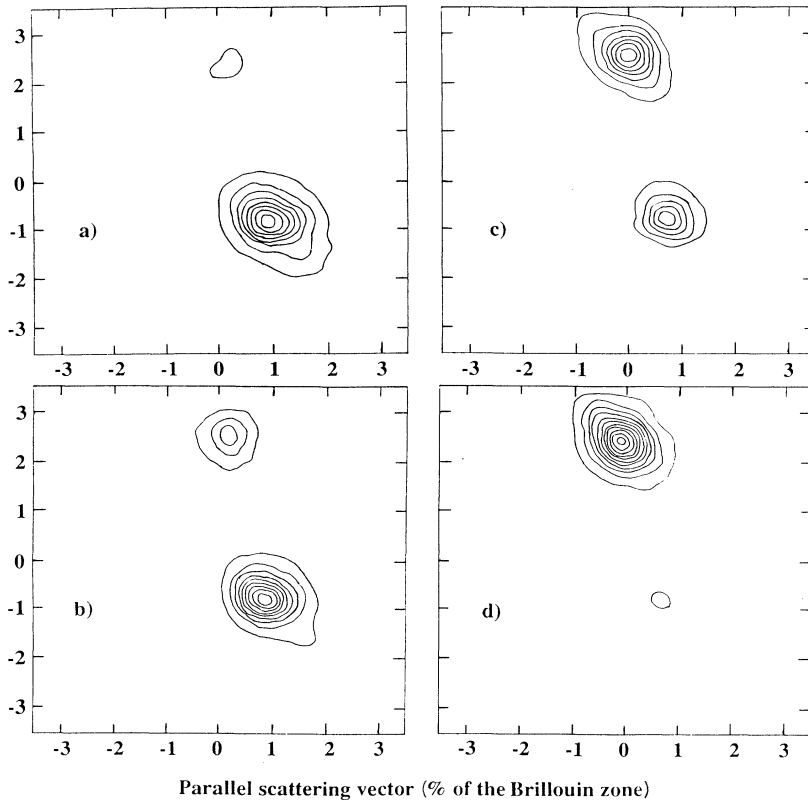


FIG. 2. A series of contour plots of the (0,0) spot intensity at a beam energy of 130 eV. The horizontal and vertical axes correspond to the $\langle 110 \rangle$ azimuths. From (a) to (d), the Cu(100) sample is moved in stages so that the incident electron beam crosses a grain boundary. The total distance, (a)–(d), is approximately 1 mm. The difference in grain orientations is approximately 1° . Comparing the contours in (c), it is apparent that the upper spot is slightly elongated, indicating limits on the average perfect-terrace size. Details such as these, which are no doubt often missed in conventional LEED studies, permit SPA-LEED data to be taken on only the most nearly perfect regions of the sample.

average perfect-terrace size. For example, the upper spot in Fig. 2(d) is more elongated than the lower spot in Fig. 2(a). Details such as these, which are no doubt often missed in conventional LEED studies, permit SPA-LEED data to be taken on only the most nearly perfect regions of the sample.

Figure 3 presents a schematic illustration of an idealization of the variation in LEED spot profile with incident electron momentum (k_\perp) for a surface with randomly spaced steps.⁴⁶ In the limit in which all atoms are found in perfect lattice sites, the spot profile varies with k_\perp from a sharp spike, reflecting long-range lattice order, to a broadened feature, reflecting the average terrace width.^{8, 13, 20, 21, 24, 31, 39, 40} The basic idea is that when terraces differing in height by an atomic step scatter the electron wave in-phase the spot-profile width is determined not by the spacing between steps but by the long-range lattice order. When the scattering is out of phase the spot-profile width is determined by average terrace size or distance between steps (or more precisely, by the Fourier transform of the autocorrelation function of surface atom positions^{6, 8, 13, 20, 21, 24, 31, 39, 41}).

In practice, deviations from the idealized illustration of Fig. 3 are found. The most noticeable one is that each symmetrically inequivalent spot has its own individual intensity-voltage relationship (I - V curve). The I - V curve is superimposed on the central spike and the broadened feature alike so that the smooth dashed and dotted envelope lines in Fig. 3 actually contain additional structure. One aspect of this additional structure is that the broadened feature is often weaker at the exact out-of-phase condition than it is slightly off the out-of-phase

condition. Since the broadened feature is generally weak at any energy (the central spike is often a factor-of-ten larger than Fig. 3 suggests), data collection is facilitated by using beam energies slightly off the out-of-phase condition. An additional advantage of this procedure is that the presence of some intensity in the sharp central spike

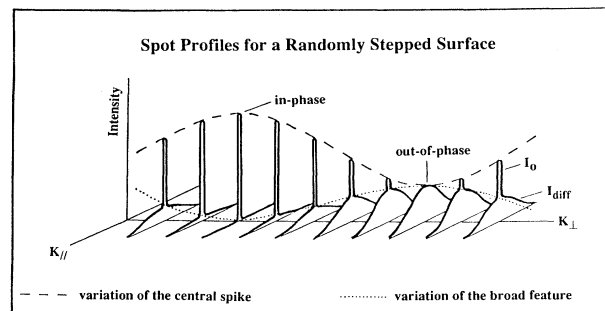


FIG. 3. An idealized schematic illustration of an observed spot profile (intensity vs in-plane scattering vector, k_\parallel) from a randomly stepped surface for different values of k_\perp ($\sim \sqrt{\text{electron energy}}$, near normal incidence). The steps split the spot into a central spike and a broadened feature. The spike dominates at values of k_\perp for which constructive interference occurs between adjacent terraces separated by a step. The width of the spike is reciprocally related to the degree of long-range lattice order. The broadened feature dominates at values of k_\perp for which destructive interference occurs between adjacent terraces separated by a step. The width of the broadened feature is reciprocally related to the average separation between steps (from Ref. 46).

greatly facilitates the alignment of the spot with the scanning axes of the SPA-LEED. Such alignment is important to ensure that single line scans pass precisely through the center of the spot.

The standard data collection procedure used in this work consisted of aligning a particular spot with the SPA-LEED and then examining the spot profile at several different beam energies in the general neighborhood of an out-of-phase condition. For the Cu(100) surface, one such out-of-phase condition occurs at around 130 eV, which turns out to be the experimentally most convenient. Profiles at lower energies suffer severely from the intensity falloffs due to the effects mentioned above, and although this problem diminishes at the higher energies, so also does the intensity of the broadened feature relative to the spike. In addition, the 130-eV beam energy enables the four (10) spots to be seen on-screen with the maximum instrumental deflection voltages, which is very convenient for setting up.

Each substantively different surface seemed to have its own optimum beam energy for displaying the broadened feature at its greatest intensity without an excessively intense central spike. While the shape and width of the broadened feature, including the Henzler rings, did not appear to depend on beam energy, the absolute intensity of these features was often very sensitive to beam energy. Large changes in absolute intensity (e.g., 50%) can occur for small changes in beam voltage (e.g., 2 eV) when trying to optimize the ratio of central-spike-to-ring intensities. Moreover, the optimum beam voltage changes by several eV with increasing deposited thickness (i.e., substantively different surfaces). Consequently, the choice we have made here of presenting 130-eV data wherever possible (in the interests of consistency) means that some of the results we present here appear more noisy than would be the case if the optimum energy had been selected for each substantively different surface.

The data reported here are plotted as a function of k_{\parallel} , the in-plane scattering vector, and are all scaled as a percentage of the width of the $\langle 011 \rangle$ Brillouin zone (k_{BZ}). This simplification avoids that confusion that might result from the different widths of the $\langle 010 \rangle$ and $\langle 011 \rangle$ zones. It has the further advantage, in the ease of inverting from reciprocal space to real space, that 10% of k_{BZ} corresponds to 10 atomic diameters (e.g., 25.5 Å for Cu).

III. RESULTS AND DISCUSSION

The first example of Henzler rings found in this work was in the Fe/Cu(100) system for deposition at 80 K. Similar rings were seen by Pappas for Fe/Cu(100) deposited at 125 K.⁷³ Figure 4 presents a typical set of single line scans for three different Fe thicknesses. The ring has a radius of $\sim 10\%$ of k_{BZ} for all three thicknesses indicating a mean separation between islands (center to center) on the order of 10 atomic diameters. This result is a typical example of a growth mode in which the density of the islands does not increase with deposited thickness;¹⁵ instead, the island density has already reached a steady state at a thickness of 0.45 monolayers (ML), and with increasing deposition, the existing islands grow in

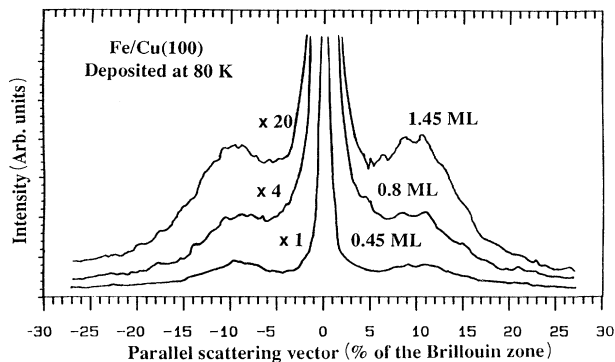


FIG. 4. Profiles in the $\langle 010 \rangle$ azimuth of the (1,0) spot for the indicated thicknesses of Fe deposited on Cu(100) at 80 K. The beam energy is 130 eV. The feature at $k_{\parallel} \sim 10\% k_{BZ}$ in all three profiles indicates that the mean separation between islands (center to center) is roughly constant at ~ 10 atomic diameters.

size until they merge and new islands nucleate on the new surface.

The results of Fig. 4 would seem difficult to account for without some degree of mobility in the deposited Fe atoms. Thermally activated diffusion can be effectively ruled out on the basis of temperature-dependent studies to be discussed shortly. It would seem that the most likely explanation is that the heat of condensation ($\sim 3-4$ eV) liberated during the condensation and accommodation process permits some very transient form of mobility that allows island formation.

It is interesting to note that the peaks corresponding to the ring are slightly more distinct (note the peak-to-valley ratio) at 0.45 and 1.45 ML than at 0.8 ML. Presumably this result indicates a tendency towards layer-by-layer growth in the sense that the island structure is less pronounced near an integral number of ML's than near a half-integral number of ML's.

It may be noted here that comparisons of the absolute intensity can be unreliable. For the data illustrated in Fig. 4 (all at 130 eV) the absolute intensity of the ring decreases with increasing Fe thickness (as the $\times 4$ and $\times 20$ imply), as the beam energy for optimum ring intensity changes by a few eV. This effect is probably best viewed as a modification in the $I-V$ curve due to a change in the details of the multiple scattering of the incident electrons. This phenomenon means that only the shape of a profile is meaningful. Since the shape of the spot profile is independent of beam energy, it appears that this type of multiple scattering effect does not have an adverse influence on the use of spot profiles for characterizing island distributions.

The three-dimensional projections of the spot intensity presented in Fig. 5 make it possible to see the complete Henzler ring for 1.2-ML Fe and to see how it changes with deposition or annealing temperature. With increased deposition or annealing temperature, the ring shows the first signs of narrowing around 225 K. At higher temperatures (e.g., 300 K), the ring collapses rapidly. This effect is a clear indication of thermally activated mobility allowing the deposited atoms to travel further so that

larger islands form at greater distances from one another. Annealing also has the expected effect of narrowing the rings. Another expected effect is that the ring is narrower for deposition at 300 K than for deposition at 100 K followed by annealing (for ~ 20 s) at 300 K. This effect is a consequence of the 300 K temperature imparting more mobility to deposited adatoms than to atoms already coalesced into islands.

The effect of annealing may be seen more clearly in the single line scans of Figs. 6 and 7. For 0.5-ML Fe films deposited at cryogenic temperatures, no substantial change occurs in the Henzler ring until near room temperature. These results indicate that the rings observed in this work behave in the expected manner with temperature, and there is thus no evidence to suggest that these rings are an artifact (i.e., not attributable to the spatial distribution of islands).

The effect of increased deposition temperature can be seen in the single line scans of Fig. 8. The ring is not observed to narrow significantly between 80 and 130 K. Above 225 K, the ring narrows rapidly. These results suggest an absence of thermally activated mobility below 130 K, a point which will be discussed later in this paper.

Figure 9 presents a three-dimensional projection of the spot intensity in which slow scans were made to provide a better image of the detail within the ring. It is apparent that four lobes of intensity appear in the $\langle 010 \rangle$ azimuths.

These lobes might suggest that the average island shape is not quite circular but has a tendency to be squared off.⁷⁴ In principal, these lobes could be accounted for by assuming that the spatial distribution of islands tended to fall into a somewhat square array, but such long-range correlations would seem less likely (in view of the expected low mobility) than some tendency for the islands to have a more short-range type of order largely in the form of island shape. A preferred island shape could be explained if atoms incident on a terrace near a downward step embed themselves in the terrace by pushing a step atom forward onto the lower terrace. A directional anisotropy to this pushing-out effect could produce islands with a preferred shape. Since a pushing out has been observed before in other systems,⁷⁵ and has been investigated theoretically,⁷⁶⁻⁸⁰ it seems plausible that such behavior may constitute at least one of the transient types of mobility needed to explain the present Fe/Cu(100) data. Note that this transient type of mobility would not account for the Henzler ring at 0.45-ML Fe in Fig. 4. At 0.45 ML very few Fe atoms will have landed on an Fe island so there is no way that a pushing-out effect could explain the indicated mean separation between islands. A different form of transient mobility involving a greater degree of horizontal mobility would be required to nucleate islands with a mean separation of on the order of 10 atomic diameters at 0.45 ML.

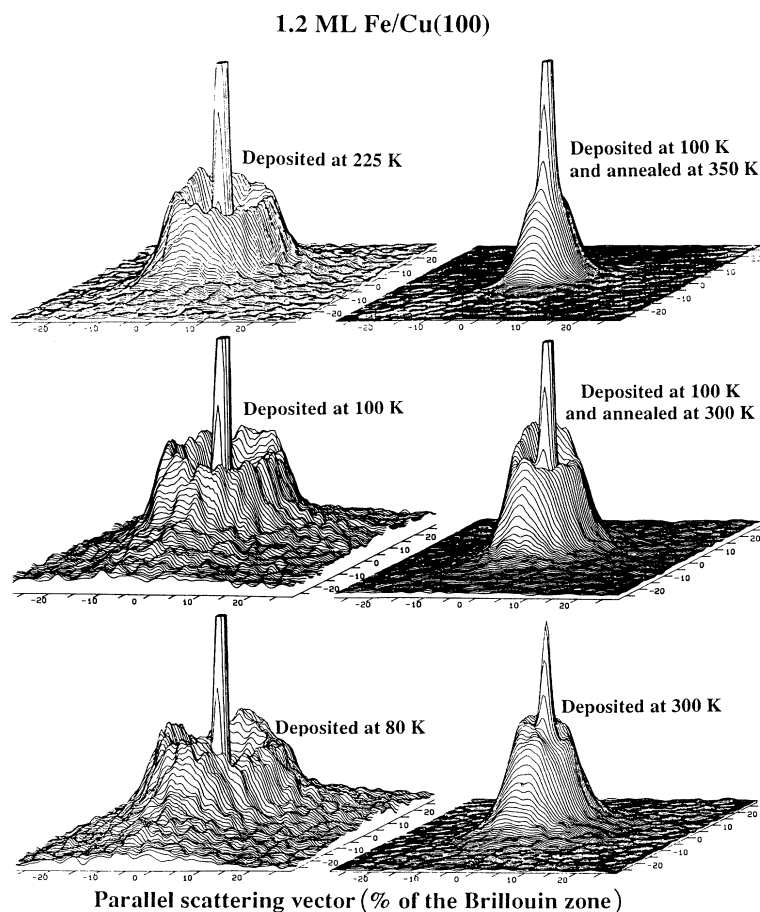


FIG. 5. An illustration of several three-dimensional projections of the (1,0) spot for 1.2-ML Fe deposited on Cu(100). The different deposition conditions (as indicated) illustrate how the ring diameter collapses with increased temperature as thermal mobility permits the growth of larger islands. In all cases the beam energy is 130 eV. The axes of the plots correspond to the $\langle 010 \rangle$ azimuths.

The deposition of Co on Cu(100) at 80 K produces Henzler rings that are almost as distinct as those produced by Fe. Figures 10 and 11 present examples of such data in the form of single line scans in both the $\langle 010 \rangle$ and $\langle 011 \rangle$ azimuths. A four-lobe structure much like that found for Fe is apparent in a comparison of the ring intensity along the two azimuths. The Co ring is less distinct than the Fe ring along the $\langle 011 \rangle$ azimuth for which Fe gives a deep minimum (e.g., Fig. 9), while Co gives a shallow one. This result suggests less uniformity in the separation between islands for Co than is the case for Fe.

A comparison of the 1.6-ML Co data in Fig. 10 at 133 eV with the 1.6-ML Co data in Fig. 11 at 129 eV provides some insight into the sensitivity of the central spike to beam energy in the general neighborhood of an out-of-phase condition. The rings are seen more clearly when the central spike is small and does not obscure the reduced intensity in the center of the ring. However, it is not always easy to make the fine adjustments to beam energy needed to obtain the spike-to-ring intensity ratio that provides an optimum display such as in Fig. 11. Moreover, a larger central spike facilitates alignment of the SPA-LEED scanning axes with the spot. Therefore,

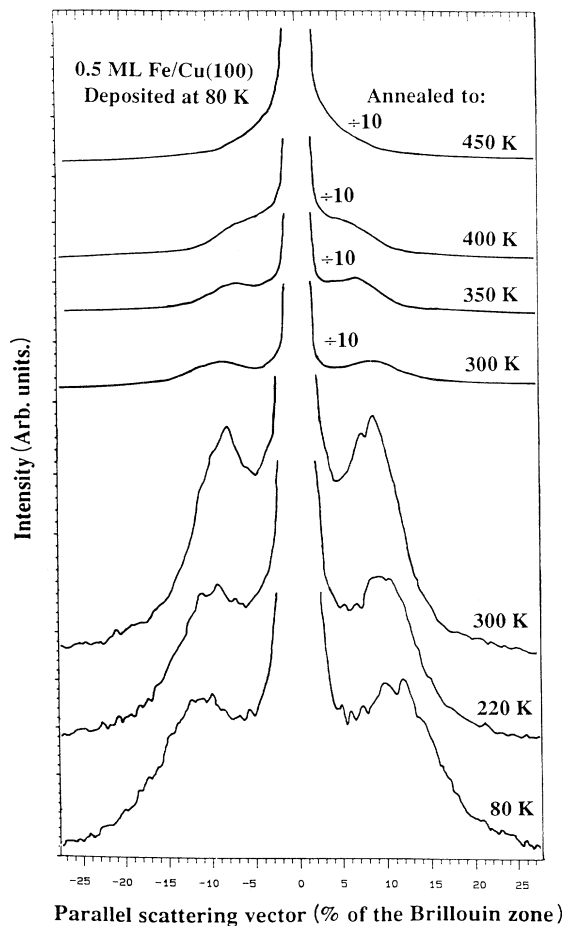


FIG. 6. Profiles in the $\langle 010 \rangle$ azimuth of the (1,0) spot for 0.5-ML Fe deposited on Cu(100) at 80 K and annealed to the indicated temperatures for ~ 20 s. The beam energy is 130 eV.

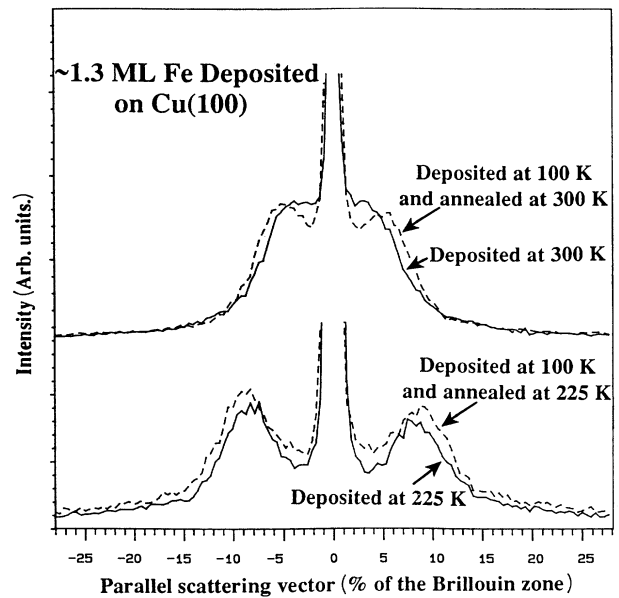


FIG. 7. Profiles in the $\langle 010 \rangle$ azimuth of the (1,0) spot for ~ 1.3 -ML Fe deposited on Cu(100) and annealed at the indicated temperatures. The results indicate that post-deposition annealing to a given temperature is less effective in narrowing the ring diameter than direct deposition at that temperature. This indicates that, as expected, free adatoms are more mobile than atoms attached to an island. The beam energy is 130 eV.

in general it is more practical to utilize a larger central spike and accept some obscuring of the reduced intensity in the center of the ring. This is a tolerable expedient because the critical issue here is the radius of the ring and the insight it provides into the spatial distribution of islands.

In the growth of Cu on Cu(100) at 80 K, the Henzler ring is not observed at the outset but develops with increasing Cu thickness and becomes very distinct by about 10 ML. Figure 12 presents a typical set of data illustrating these points. At 0.5 ML no ring is observed (although the central spike could mask a weak central minimum in the intensity), and the broadened feature appears to have a full width at half maximum of $\sim 25\%$ k_{BZ} .⁸¹ Since the analog of the radius of the ring is the halfwidth at half-maximum for a simple broadened spot,¹² the data imply a mean separation between islands of ~ 8 atoms, a value somewhat less than that found for Fe, and implies a broader distribution of island separations than was the case for Fe. The implication of this result is that less transient mobility is required to account for the 0.5-ML data of Cu than of Fe.

The dependence of the ring diameter on deposition temperature may be seen in Fig. 13. The first faint sign of a contraction in radius with increasing temperature occurs at 150 K. Above that temperature the radius shrinks rapidly. This behavior parallels that in the Co and Fe on Cu(100) systems, in which thermally activated diffusion at elevated temperatures produces larger islands with a greater separation between them.

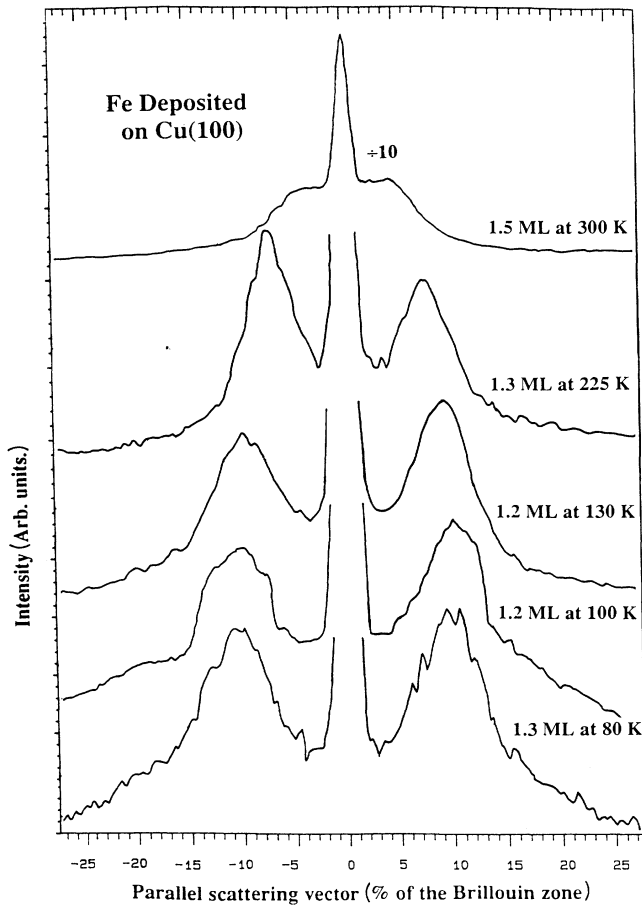


FIG. 8. Profiles in the $\langle 010 \rangle$ azimuth of the (1,0) spot for the indicated thicknesses of Fe deposited on Cu (100) at the indicated temperatures. The beam energy is 130 eV.

The Henzler ring produced by the Cu/Cu(100) system also exhibits a four-lobe structure very much like that shown in Fig. 9 for Fe. A three-dimensional projection of this pattern is given in Fig. 14 for 150-K deposition. This temperature was the highest deposition temperature that resulted in the four-lobe structure. Higher temperatures, at which thermally activated diffusion should play a significant role, yielded rings which were of more uniform intensity around their tops. Likewise, gentle thermal annealing of samples exhibiting rings with the four lobes caused the lobes to smooth out into a ring of more uniform intensity. These results suggest that the somewhat squared-off island shapes, which the lobes would seem to suggest, are not the equilibrium island shape, and that thermal diffusion leads to more circular island shapes.

As in the case of Fe/Cu(100), the four-lobe structure for the 9.5-ML Cu/Cu(100) system may be in part a reflection of a growth mechanism in which the heat of condensation allows a Cu atom landing on the upper terrace near a step to embed itself in the terrace by pushing out a step atom onto the lower terrace. However, as in the case of Co and Fe on Cu(100), the radius of the ring is large enough (10% of k_{BZ}) so that it would seem unlikely that this transient form of mobility can alone account for the data and other forms of transient forms of mobility seem likely.

It is interesting that there has been an observation of a four-lobe structure for deposition of 0.5-ML Cu/Cu(100).⁵³ However, this work differs from ours in that the deposition temperature was 300 K, and the ring had a much smaller radius.⁵³ The smaller radius would seem to be a consequence thermal diffusion giving a larger mean separation between islands. The observation of the four lobes at 300 K is harder to understand since we did not observe lobes for deposition temperatures above 150 K in our 9.5-ML Cu films.

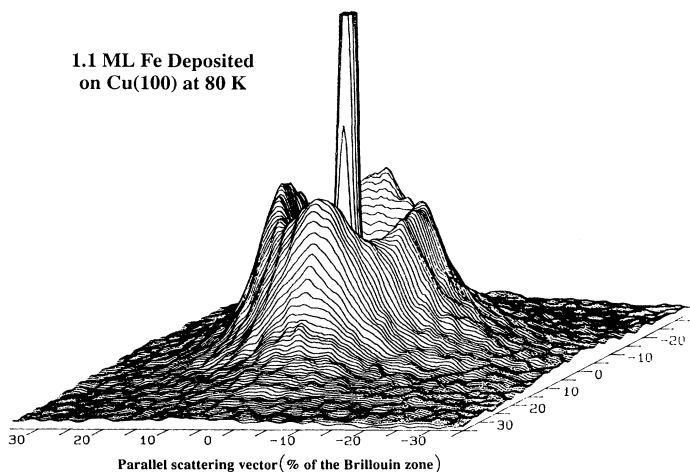


FIG. 9. An illustration of a three-dimensional projection of the (1,0) spot for 1.1-ML Fe deposited on Cu(100) at 80 K. The improved signal-to-noise ratio compared to Fig. 5 is the result of a fivefold reduction in scan rate. The beam energy is 130 eV. The axes of the plot correspond to the $\langle 010 \rangle$ azimuths.

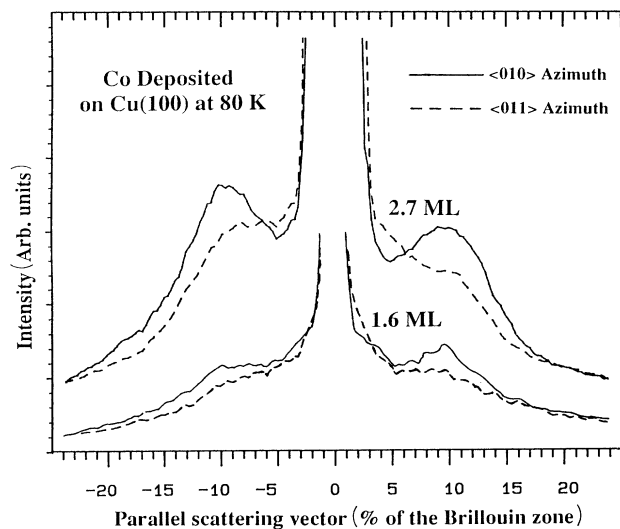


FIG. 10. Profiles in the $\langle 010 \rangle$ and $\langle 011 \rangle$ azimuths of the $(1,0)$ spot for 1.6-ML Co (at a beam energy of 133 eV) and 2.7-ML Co (at a beam energy of 155 eV) deposited on Cu(100) at 80 K. The greater intensity of the ring in the $\langle 010 \rangle$ azimuth indicates the presence of four lobes with the same orientation as in Fig. 9.

One final point of interest in this work is the issue of the temperature dependence of the thermally activated diffusion of the deposited atoms. Many readers will wish to know what the hopping rate (from site to site) is for a Cu adatom on Cu(100) at 80 K. Experimental determinations of the activation energy for this process have produced values of 0.48,⁸² 0.39,⁶¹ and 0.28 eV.⁵⁴ The smallest estimate comes from an Arrhenius plot by Ernst, Fabre, and Lapujoulade⁵⁴ of the log of the mean island separation versus the reciprocal of the deposition temperature. This plot has been reproduced in Fig. 15, and additional data from the present work have been included for comparison. All three plots in Fig. 15 suggest that the

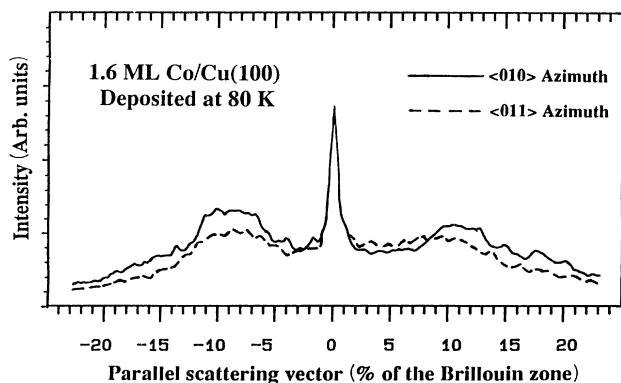


FIG. 11. Profiles in the $\langle 010 \rangle$ and $\langle 011 \rangle$ azimuths of the $(1,0)$ spot for 1.6-ML Co deposited on Cu(100) at 80 K. The greater intensity of the ring in the $\langle 010 \rangle$ azimuth indicates the presence of four lobes with the same orientation as in Figs. 9. The beam energy is 129 eV.

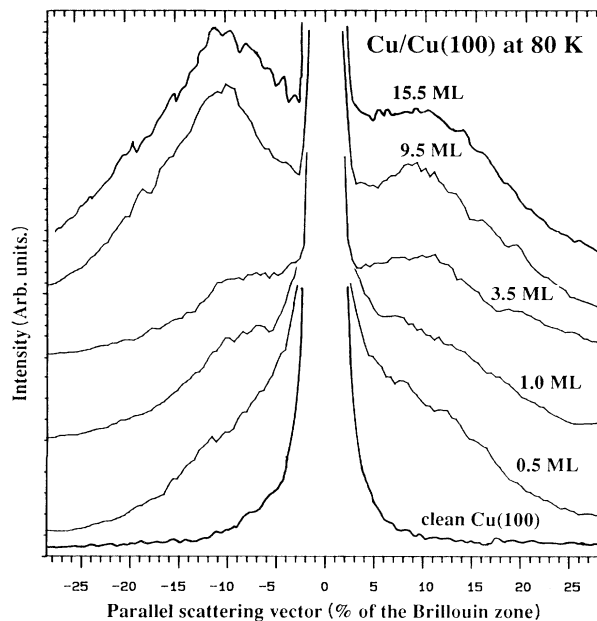


FIG. 12. Profiles in the $\langle 010 \rangle$ azimuth of the $(1,0)$ spot for the indicated thicknesses of Cu deposited on Cu(100) at 80 K. The beam energies are 125 eV for all except the 9.5-ML Cu film (133 eV) and the 15.5-ML Cu film (137 eV). Note that the ring intensities on the left and right of the central peak are not necessarily of equal intensity because the sides are not symmetrically equivalent, the one on the left being closer to the $(0,0)$ spot than the one on the right.

onset of a significant rate of thermal diffusion occurs at around 150 K or above. The data of Ernst, Fabre, and Lapujoulade suggest somewhat larger island separations than our data, but their data are based on He diffraction, and this difference could be a result of the different techniques used. Ernst, Fabre, and Lapujoulade extracted the 0.28-eV activation energy from their Arrhenius plot. They estimated the pre-exponential factor to be 10^{-5} cm²/s.⁵⁴ Using these values, the hopping rate for a Cu adatom is predicted to be 1 hop/s at 138 K, and at 80 K the time between hops is predicted to be about one year. Since the deposition rate in this work is about 3 ML/min, it is reasonable for the effects of thermally activated diffusion to become apparent around and above 150 K. Therefore, it seems safe to conclude that any hopping of Cu adatoms that occurs for deposition at 80 K is a transient effect associated with the condensation and accommodation process and not a result of thermally activated diffusion.

IV. CONCLUSIONS

The major conclusions of this work may be summarized as follows.

(1) Thin epitaxial films of Fe, Co, and Cu on Cu(100) deposited at 80 K exhibit rings around the substrate LEED spots with a radius of $\sim 10\%$ k_{BZ} . The rings are apparent for thicknesses as small as 0.45 ML for Fe, but develop more gradually for Cu.

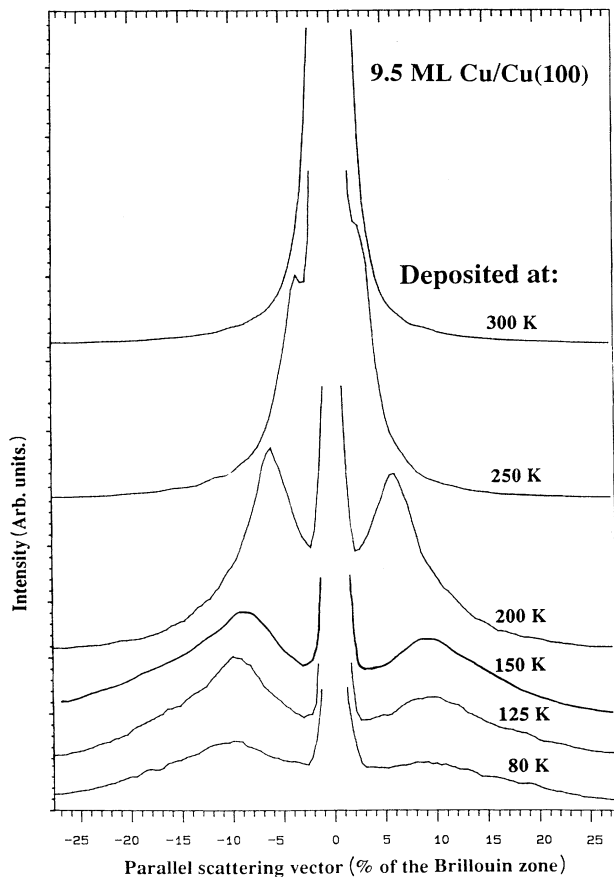


FIG. 13. Profiles in the $\langle 010 \rangle$ azimuth of the (1,0) spot for 9.5-ML Cu deposited on Cu(100) at the indicated temperatures. After deposition the sample was cooled to 80 K for data collection. The beam energies are 133 eV for all data (except for the 125-K data for which the energy is 135 eV).

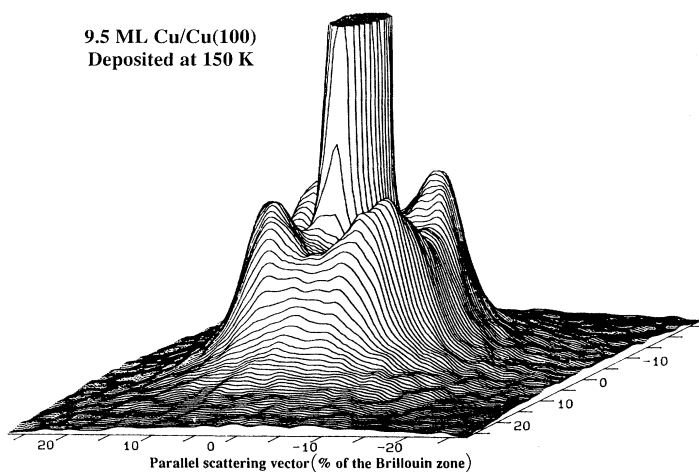


FIG. 14. An illustration of a three-dimensional projection of the (1,0) spot for 9.5-ML Cu deposited on Cu(100) at 150 K. This temperature is near the upper limit for which the four lobes can be observed. Higher deposition temperatures permit enough thermal mobility of adatoms to give a ring of more uniform intensity. The beam energy is 130 eV. Note that the four lobes appear in the same azimuths as in Fig. 9 since in the present figure the axes of the plot correspond to the $\langle 011 \rangle$ azimuths.

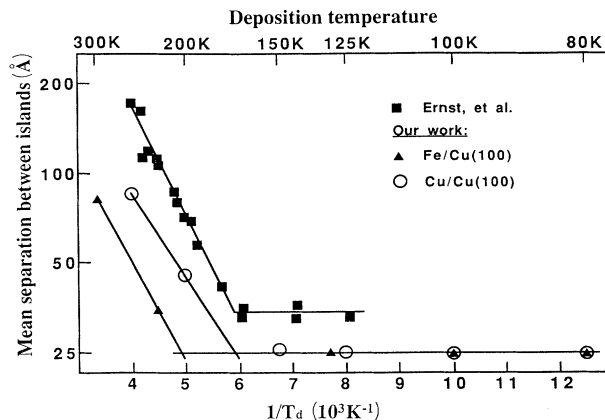


FIG. 15. Plots of the mean separation between islands vs the reciprocal of the absolute deposition temperature (adapted from Ref. 54). The data from Ernst, Fabre, and Lapujoulade (Ref. 54) are for Cu on Cu(100) as measured by He diffraction. All three data sets indicate that the onset of thermally activated mobility is above about 150 K, so that 80 K should be low enough to suppress completely any mobility except that connected with the impact and accommodation processes.

(2) These rings indicate a mean island separation on the order of 10 atomic diameters, implying that the deposited atoms do not come to rest at the site of impact. The rings could be accounted for by assuming that some transient form of mobility is associated with the condensation and accommodation process.

(3) The rings behave in the expected manner with temperature. Elevated deposition temperatures or annealing produce smaller rings as thermally activated diffusion produced larger islands with a greater mean separation.

(4) The rings exhibit a four-lobe structure that might

suggest the islands have a somewhat squared-off shape as deposited. Upon annealing to the onset of thermally activated diffusion, these lobes disappear indicating that the equilibrium island shape is nearly circular.

(5) Thermally activated diffusion becomes apparent in the present data around or above ~ 150 K and appears to be strongly suppressed for deposition at 80 K.

(6) The SPA-LEED data on these systems is generally consistent with the available STM results.⁷⁰

(7) In the literature, there do not appear to be any

molecular-dynamics simulations of the present epitaxial systems which account for the rings observed in this work. The present data should be a challenging test for such calculations in the future.

ACKNOWLEDGMENTS

The authors are pleased to acknowledge valuable discussions with Dr. J. W. Evans, Dr. P. A. Thiel, Dr. A. E. DePristo, Dr. D. P. Pappas, and Dr. J. F. Wendelken.

*Permanent address: Chemistry Department, La Trobe University, Bundoora, Australia 3083.

¹R. L. Park, *J. Appl. Phys.* **37**, 295 (1966).

²R. L. Park, in *Proceedings of the 4th International Materials Symposium*, edited by G. A. Somorjai (Wiley, New York, 1969), p. 28.

³J. C. Tracy and J. M. Blakely, in *Proceedings of the 4th International Materials Symposium* (Ref. 2), p. 65.

⁴W. P. Ellis and R. L. Schwoebel, *Surf. Sci.* **11**, 82 (1968).

⁵M. Henzler, *Surf. Sci.* **19**, 159 (1970).

⁶J. E. Houston and R. L. Park, *Surf. Sci.* **21**, 209 (1970); **26**, 269 (1971).

⁷M. Henzler, *Appl. Phys.* **9**, 11 (1976).

⁸M. Henzler, in *Electron Spectroscopy for Surface Analysis*, edited by H. Ibach (Springer, Berlin, 1977), p. 117.

⁹J. M. Cowley and H. Schuman, *Surf. Sci.* **38**, 53 (1977).

¹⁰D. Wolf, H. Jagodzinski, and W. Moritz, *Surf. Sci.* **77**, 283 (1978).

¹¹H. Jagodzinski, W. Moritz, and D. Wolf, *Surf. Sci.* **77**, 233 (1978); **77**, 249 (1978); **77**, 265 (1978); **77**, 283 (1978).

¹²M. Henzler, *Surf. Sci.* **73**, 240 (1978).

¹³M. Henzler, in *Festkörperprobleme XIX*, edited by J. Treusch (Verweg, Braunschweig, 1979), p. 193.

¹⁴T. M. Lu and M. G. Lagally, *J. Vac. Sci. Technol.* **17**, 207 (1980); *Surf. Sci.* **120**, 47 (1982).

¹⁵P. Hahn, J. Clabes, and M. Henzler, *J. Appl. Phys.* **51**, 2079 (1980).

¹⁶D. G. Welkie, M. G. Lagally, and R. L. Palmer, *J. Vac. Sci. Technol.* **17**, 453 (1980).

¹⁷J. Lapujoulade, *Surf. Sci.* **108**, 526 (1981).

¹⁸E. D. Williams and W. H. Weinberg, *Surf. Sci.* **109**, 574 (1981).

¹⁹T.-M. Lu, G.-C. Wang, and M. G. Lagally, *Surf. Sci.* **108**, 494 (1981).

²⁰M. Henzler, *Appl. Surf. Sci.* **11/12**, 450 (1982).

²¹M. G. Lagally, *Appl. Surf. Sci.* **13**, 260 (1982).

²²K. D. Gronwald and M. Henzler, *Surf. Sci.* **117**, 180 (1982).

²³M. Henzler, *Surf. Sci.* **132**, 82 (1982).

²⁴M. Henzler, *Appl. Phys. A* **34**, 205 (1984).

²⁵M. R. Presicci and T.-M. Lu, *Surf. Sci.* **141**, 233 (1984).

²⁶C. S. Lent and P. I. Cohen, *Surf. Sci.* **139**, 121 (1984); *J. Vac. Sci. Technol. A* **2**, 861 (1984).

²⁷J. M. Pimbley and T.-M. Lu, *J. Appl. Phys.* **55**, 182 (1984); **57**, 1121 (1985); **58**, 2184 (1986); *J. Vac. Sci. Technol. A* **2**, 457 (1984); *Surf. Sci.* **139**, 360 (1984).

²⁸D. Saloner and M. G. Lagally, *J. Vac. Sci. Technol. A* **2**, 935 (1984); in *Advanced Photon and Particle Techniques for the Characterization of Defects in Solids*, edited by J. B. Roberto, R. W. Carpenter, and M. C. Wittels, MRS Symposia Proceedings No. 41 (Materials Research Society, Pittsburgh, 1985), p.

179; *Surf. Sci.* **26**, 418 (1986); in *The Structure of Surfaces*, edited by M. A. Van Hove and S. Y. Tong (Springer, New York, 1985), p. 366.

²⁹M. Henzler, *Surf. Sci.* **152/153**, 963 (1985).

³⁰H. Busch and M. Henzler, *Surf. Sci.* **167**, 534 (1986).

³¹M. Henzler, in *Dynamical Phenomena at Surfaces, Interfaces, and Superlattices*, edited by F. Nizzili, K. H. Rieder, and R. F. Willis (Springer, Berlin, 1986), p. 11.

³²P. Heilmann, E. Lang, K. Heinz, and K. Müller, *Appl. Phys.* **9**, 247 (1976).

³³P. C. Stair, *Rev. Sci. Instrum.* **51**, 132 (1980).

³⁴U. Scheithauer, G. Meyer, and M. Henzler, *Surf. Sci.* **178**, 441 (1986).

³⁵M. G. Lagally and J. A. Martin, *Rev. Sci. Instrum.* **54**, 1273 (1983).

³⁶E. G. McRae, R. A. Malic, and D. A. Kapilow, *Rev. Sci. Instrum.* **56**, 2077 (1985).

³⁷R. Q. Hwang, E. D. Williams, and R. L. Park, *Rev. Sci. Instrum.* **60**, 2945 (1989).

³⁸M. Horn and M. Henzler, *J. Crystal. Growth* **81**, 428 (1987).

³⁹M. G. Lagally, D. E. Savage, and M. C. Tringides, in *Reflection High-energy Electron Diffraction and Reflection Electron Imaging of Surfaces*, edited by P. K. Larsen and P. J. Dobson (Plenum, New York, 1988), p. 163.

⁴⁰M. Henzler, in *The Structure of Surfaces II*, edited by J. F. van der Veen and M. A. Van Hove (Springer, Berlin, 1988), p. 431.

⁴¹R. Kariotis, D. E. Savage, and M. G. Lagally, *Surf. Sci.* **204**, 491 (1988).

⁴²G. Meyer, M. Michailov, and M. Henzler, *Surf. Sci.* **202**, 125 (1988).

⁴³R. Altsinger, H. Busch, M. Horn, and M. Henzler, *Surf. Sci.* **200**, 235 (1988).

⁴⁴D. W. Kruger, D. E. Savage, and M. G. Lagally, *Phys. Rev. Lett.* **63**, 402 (1989).

⁴⁵G. Meyer, J. Wollschläger, and M. Henzler, *Surf. Sci.* **231**, 64 (1990).

⁴⁶J. Wollschläger, J. Falta, and M. Henzler, *Appl. Phys. A* **50**, 57 (1990).

⁴⁷M. Henzler, H. Busch, and G. Friese, in *Kinetics of Ordering and Growth at Surfaces*, edited by M. G. Lagally (Plenum, New York, 1990), p. 101.

⁴⁸M. Henzler, in *Kinetics of Ordering and Growth at Surfaces* (Ref. 47), p. 193.

⁴⁹W. Moritz, in *Kinetics of Ordering and Growth at Surfaces* (Ref. 47), p. 175.

⁵⁰G. Meyer, J. Wollschläger, and M. Henzler, *Surf. Sci.* **231**, 64 (1990).

⁵¹S. Heun, J. Falta, and M. Henzler, *Surf. Sci.* **243**, 132 (1991).

⁵²J.-K. Zuo and J. F. Wendelken, *J. Vac. Sci. Technol. A* **9**,

- 1539 (1991); *Appl. Surf. Sci.* **48/49**, 366 (1991); *Phys. Rev. Lett.* **66**, 2227 (1991).
- ⁵³J.-K. Zuo and J. F. Wendelken, *Phys. Rev. Lett.* **70**, 1662 (1993); and (unpublished).
- ⁵⁴H.-J. Ernst, F. Fabre, and J. Lapujoulade, *Surf. Sci.* **275**, L687 (1992); *Phys. Rev. B* **46**, 1929 (1992).
- ⁵⁵Y.-L. He and G.-C. Wang, in *Interface Dynamics and Growth*, edited by K. S. Liang, M. P. Anderson, R. F. Bruinsma, and G. Scoles, MRS Symposia Proceedings No. 237 (Materials Research Society, Pittsburgh, 1992), p. 429; and (unpublished).
- ⁵⁶Y.-F. Liew, Y.-L. He, A. Chan, and G.-C. Wang, *Surf. Sci.* **273**, L461 (1992).
- ⁵⁷K. R. Roos and M. C. Tringides, *Phys. Rev. B* **47**, 12 705 (1993); *Surf. Sci.* (to be published); *Europhys. Lett.* **23**, 257 (1993); R. Biswas, K. Roos, and M. C. Tringides, in *Common Themes and Mechanisms of Epitaxial Growth*, edited by P. Fuoss, D. W. Kisker, J. Tsao, and A. Zangwill (Materials Research Society, Pittsburgh, in press).
- ⁵⁸R. D. Young and D. C. Schubert, *J. Chem. Phys.* **42**, 3943 (1965).
- ⁵⁹J. W. Evans, D. E. Sanders, P. A. Thiel, and A. E. DePristo, *Phys. Rev. B* **41**, 5410 (1990); H. C. Kang, D. K. Flynn-Sanders, P. A. Thiel, and J. W. Evans, *Surf. Sci.* **256**, 205 (1991); D. K. Flynn-Sanders, J. W. Evans, and P. A. Thiel, *ibid.* **289**, 75 (1993).
- ⁶⁰W. F. Egelhoff, Jr. and I. Jacob, *Phys. Rev. Lett.* **62**, 921 (1989).
- ⁶¹M. Breeman and D. O. Boerma, *Phys. Rev. B* **46**, 1703 (1992).
- ⁶²M. Schneider, A. Rahman, and I. K. Schuller, *Phys. Rev. Lett.* **55**, 604 (1985).
- ⁶³M. Schneider, A. Rahman, and I. K. Schuller, *Superlat. Microstruct.* **7**, 39 (1990).
- ⁶⁴D. E. Sanders and A. E. DePristo, *Surf. Sci.* **254**, 341 (1991).
- ⁶⁵D. E. Sanders, D. M. Halstead, and A. E. DePristo, *J. Vac. Sci. Technol. A* **10**, 1986 (1992).
- ⁶⁶C. M. Gilmore and J. A. Sprague, *J. Vac. Sci. Technol. A* **10**, 1597 (1992).
- ⁶⁷J. A. Sprague and C. M. Gilmore, in *Material Modification by Energetic Atoms and Ions*, edited by K. S. Grabowski, S. A. Barnett, S. M. Rossvogel, and K. Wasa, MRS Symposia Proceedings No. 268 (Materials Research Society, Pittsburgh, in press).
- ⁶⁸P. S. Weiss and D. M. Eigler, *Phys. Rev. Lett.* **69**, 2240 (1992).
- ⁶⁹S. S. Parkin, Z. G. Li, and K. J. Smith, *Appl. Phys. Lett.* **58**, 2710 (1991); D. H. Mosca, F. Petroff, A. Fert, P. A. Schroeder, W. P. Pratt, Jr., and R. Laloe, *J. Magn. Mater.* **94**, L1 (1991); J. J. de Miguel, A. Cebollada, J. M. Gallego, R. Miranda, C. M. Schneider, P. Schuster, and J. Kirschner, *ibid.* **93**, 1 (1991); B. Dieny, V. S. Speriosu, S. S. P. Parkin, B. A. Gurney, D. R. Wilhoit, and D. Mauri, *Phys. Rev. B* **43**, 1297 (1991); W. R. Bennett, W. Schwarzacher, and W. F. Egelhoff, Jr., *Phys. Rev. Lett.* **65**, 3169 (1990).
- ⁷⁰D. D. Chambliss, R. J. Wilson, and S. Chiang, *J. Vac. Sci. Technol. A* **10**, 1993 (1992); K. E. Johnson, D. D. Chambliss, R. J. Wilson, and S. Chiang, *ibid.* **11**, 1654 (1993); A. Brodde and H. Neddermeyer, *Surf. Sci.* **287/288**, 988 (1993); A. K. Schmidt, D. Atlan, H. Itoh, B. Heinrich, T. Ichinokawa, and J. Kirschner (unpublished).
- ⁷¹W. F. Egelhoff, Jr., I. Jacob, J. M. Rudd, J. F. Cochran, and B. Heinrich, *J. Vac. Sci. Technol. A* **8**, 1582 (1990); W. F. Egelhoff, in *Layered Structures, Epitaxy, and Interfaces*, edited by J. M. Gibson and L. R. Dawson, MRS Symposia Proceedings No. 37 (Materials Research Society, Pittsburgh, 1985), p. 443; in *Physical and Chemical Properties of Thin Metal Overlayers and Alloy Surfaces*, edited by D. M. Zehner and D. W. Goodman, MRS Symposia Proceedings No. 83 (Materials Research Society, Pittsburgh, 1987), p. 189; D. A. Steigerwald, I. Jacob, and W. F. Egelhoff, Jr., *Surf. Sci.* **202**, 472 (1988); D. A. Steigerwald and W. F. Egelhoff, Jr., *J. Vac. Sci. Technol. A* **7**, 3123 (1989); M. T. Kief and W. F. Egelhoff, Jr., *Phys. Rev. B* **47**, 10 785 (1993).
- ⁷²J. S. Ahearn, Jr., J. P. Monaghan, Jr., and J. W. Mitchell, *Rev. Sci. Instrum.* **41**, 1853 (1970).
- ⁷³D. P. Pappas, Ph.D. thesis, University of California, Irvine, CA, p. 34.
- ⁷⁴M. C. Bartlet and J. W. Evans, in *Proceedings of the US-Japan Conference on Surface Characterization*, edited by P. I. Cohen and A. Ichimiya [*Surf. Sci.* (to be published)].
- ⁷⁵S. C. Wang and G. Ehrlich, *Phys. Rev. Lett.* **67**, 2509 (1992).
- ⁷⁶D. M. Halstead and A. E. DePristo, *Surf. Sci.* **286**, 275 (1993); P. Stoltze and J. K. Nørskov, *Phys. Rev. B* **48**, 5607 (1993).
- ⁷⁷J. W. Evans, *Phys. Rev. B* **43**, 3897 (1991).
- ⁷⁸H. C. Kang and J. W. Evans, *Surf. Sci.* **271**, 321 (1992).
- ⁷⁹J. W. Evans and M. C. Bartlet, *Surf. Sci. Lett.* **284**, L437 (1993).
- ⁸⁰D. E. Sanders and J. W. Evans, in *The Structure of Surfaces III*, edited by S. Y. Tong, M. A. Van Hove, X. Xide, and K. Takayanagi (Springer-Verlag, Berlin, 1991), p. 38.
- ⁸¹Note here that, as explained in Sec. II, this width is scaled for simplicity as a percentage of the $\langle 011 \rangle$ Brillouin-zone width. If it were scaled as a percentage of the $\langle 010 \rangle$ Brillouin-zone width the 25% value would become 17.7%.
- ⁸²J. J. de Miguel, A. Cebollada, J. M. Gallego, J. Ferrón, and S. Ferrer, *J. Crystal. Growth* **88**, 442 (1988).